3. 1. 2. 3 MEBT1

The medium-energy beam-transport line (MEBT) from the RFQ to the DTL has been constructed according to the JHF design [1, 2]. The first beam of about 10 mA was successfully transmitted through the line with a nearly 100% transmission ratio by some tuning of the magnetic field gradient of the focusing magnets. Figure 3.1.2.3.1 shows the MEBT installed into the tunnel at the KEK. The layout is shown in Fig. 2.1.3.1.2 and the parameters of MEBT1 are listed in Table 2.1.3.1.1 in section 2.1.3.1. The MEBT is to be utilized as MEBT1 in the joint project.

3. 1. 2. 3. 1 Buncher

A re-entrant-type single cavity was chosen for the buncher [2], since stable operation can be expected owing to its simple geometry. The main parameters of the buncher are listed in Table 3.1.2.3.1. The required rf pulse length is 600 μsec with a 50 Hz repetition rate. After machining a half part of the cavity from OFHC copper (Fig. 3.1.2.3.2), two of them were brazed together. An unloaded Q-value of more than 27000 was obtained. The cavities were successfully driven up to an rf input power of 10 kW without any discharge problems. Two automatic controlled tuners were prepared for tuning resonant frequency.

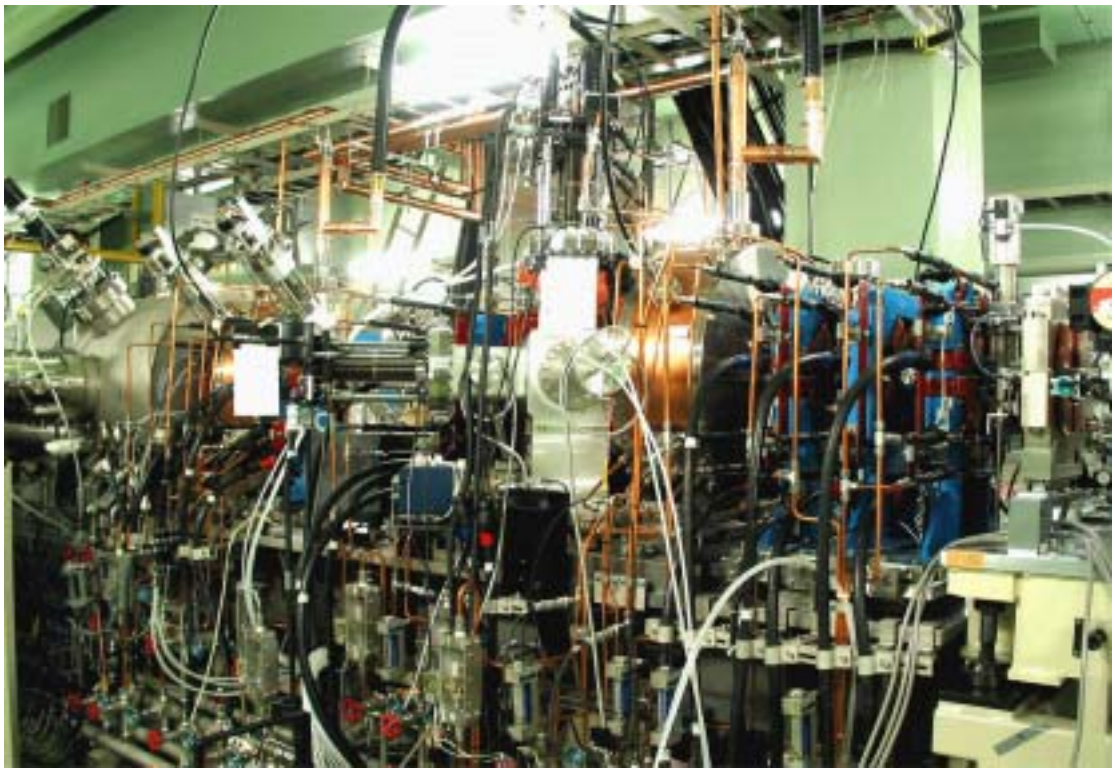

Fig. 3.1.2.3.1 Photograph of the MEBT installed at KEK.

Table 3.1.2.3.1 Parameters of the buncher and the chopper.

	Buncher	chopper	
Frequency	324	324	MHz
Cavity length	159.12	172	mm
Cavity diameter	564.55	326	mm
Bore radius	13	10	mm
Gap length	13	20	mm
Nose cone angle	20		degree
Quality factor	27540	11000 (Q_L ~ 10 – 15)	
Shunt impedance	40.2	4.87	MΩ/m
Transit time factor	0.694		
Input Power	7.6	18 – 27	kW
Accelerating field	3.0	1.6	MV/m
Maximum surface field	1.2	0.09	Kilpatrick

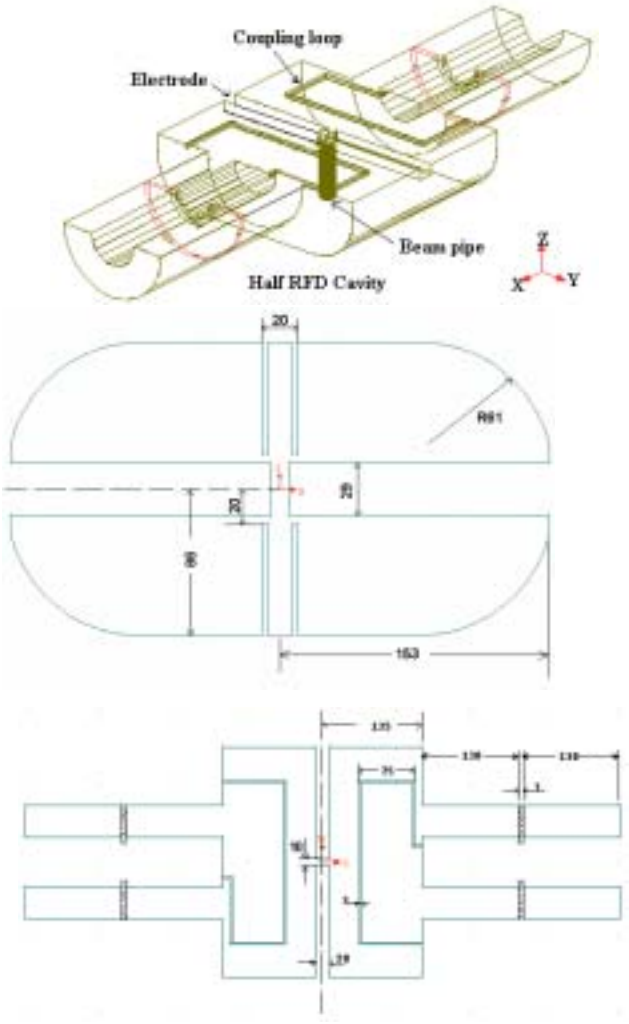

Fig. 3.1.2.3.3 Geometry of the RFD.

Fig. 3.1.2.3.2 A half part of the buncher cavity before brazing.

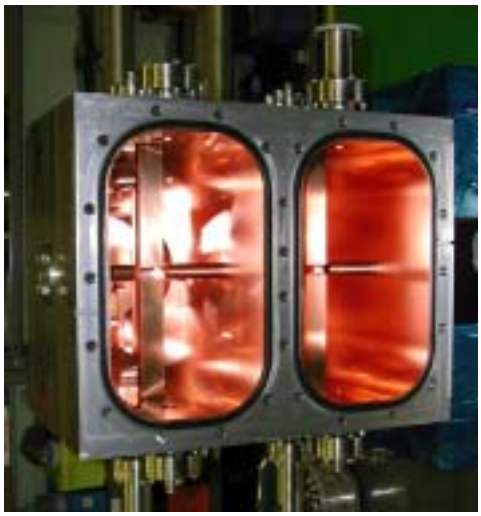

Fig. 3.1.2.3.4 Photograph of two RFD cavities.

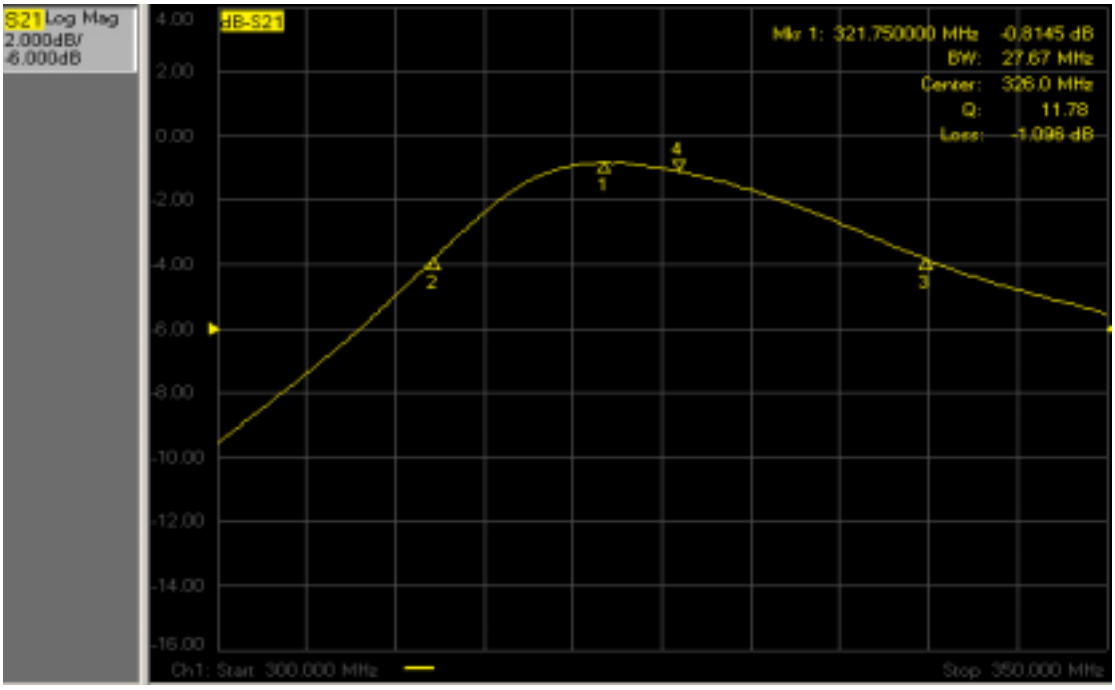

Fig. 3.1.2.3.5 Measured frequency spectrum of the single RFD.

3. 1. 2. 3. 2 Chopper

An rf chopper (RFD) was proposed for chopping the proton beam in the low-energy region [3]. There are two factors for determining the rise time of the deflecting field: loaded Q-value of the RFD and the rise time of the rf power amplifier. The cavity design was improved by both experimental and calculated studies [1, 4]. The main parameters are listed in Table 3.1.2.3.1. HFSS was also used for designing the RFD with large rf coupling loops. Figure 3.1.2.3.3 shows the geometry of the RFD. Two RFD (RFD-A and RFD-B) were constructed as a whole (Fig. 3.1.2.3.4). It was made of stainless steel and electroplated with copper (0.1 mm in thickness).

Low-level rf measurements

(a) Measurement of the RFD with small coupling loops

The fundamental rf properties were measured by using two flat end-plates and small rf monitors, instead of using large coupling loops. Table 3.1.2.3.2 lists the measured frequencies and the unloaded Q-values. Mode 1 denotes the deflecting mode. Since the calculated Q-value is about 11000, the obtained results were satisfactory.

Table 3.1.2.3.2 Results of low-level rf measurements.

	RFD- A		RFD- B	
	Frequency(MHz)	Q	Frequency(MHz)	Q
Small loop				
Mode 1	322.275	9760	321.849	9720
Mode 2	401.916	9520	402.118	9800
Mode 3	930.349	11500	930.526	13500
Mode 4	992.514	26700	992.255	27200
Large loop				
Mode 1	323.81	11	323.88	11

(b) Measurement of the RFD with large coupling loops

To obtain a very fast rising/falling time, two large coupling loops are used in the RFD. Figure 3.1.2.3.5 shows the spectrum of the single RFD with large coupling loops. The measured band width of the single RFD is about 30 MHz. A loaded Q-value of 11 was achieved, corresponding to a rising time of 11 ns.

High-power test of the single RFD

A 30-kW rf power amplifier with a rising time of less than 15 nsec was successfully constructed (section 3.1.3.7 in this report). A high-power test of the RFD was performed. The RFD works well without any discharge under a 30-kW peak input power of 600-μsec pulse duration with a repetition rate of 50 Hz. Figure 3.1.2.3.6 shows the field amplitude in the RFD with a 30 kW input power. The variation of the temperature of the cavity, cooled by some amount of water, was less than 0.3 degrees during a high-power test. The achieved rising time, defined from 10 to 90% of the design field, is about 15 nsec.

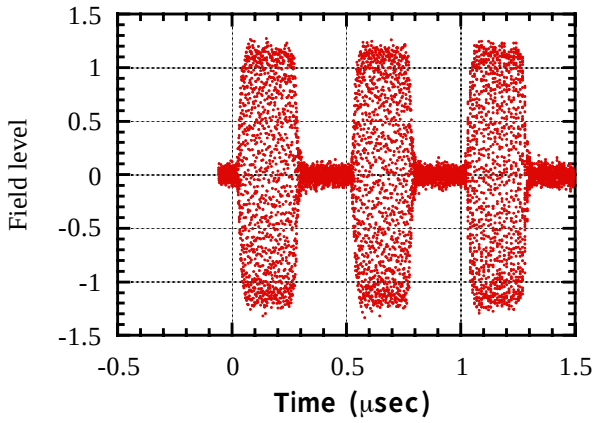

Fig. 3.1.2.3.6 RF field amplitude in the single RFD with a 30 kW input power.

Measurement of a coupled RFD

A coupled RFD system was proposed [4]. If two RFD cavities are connected so that the output power from the first RFD is utilized for the second one, the total RF power required for the two cavities may be halved, since the loaded Q-value of the RFD is very low. Comparing with HFSS simulations, a measurement of the coupled system was performed. Two cavities are connected with a 39D coaxial cable. The cable length must be chosen correctly so that the phase advance of the deflection field between two cavities is $2n\pi$.

The cable length was determined according to the results of a HFSS simulation. Figure 3.1.2.3.7 shows the measured spectrum of the coupled RFD system. The agreement between

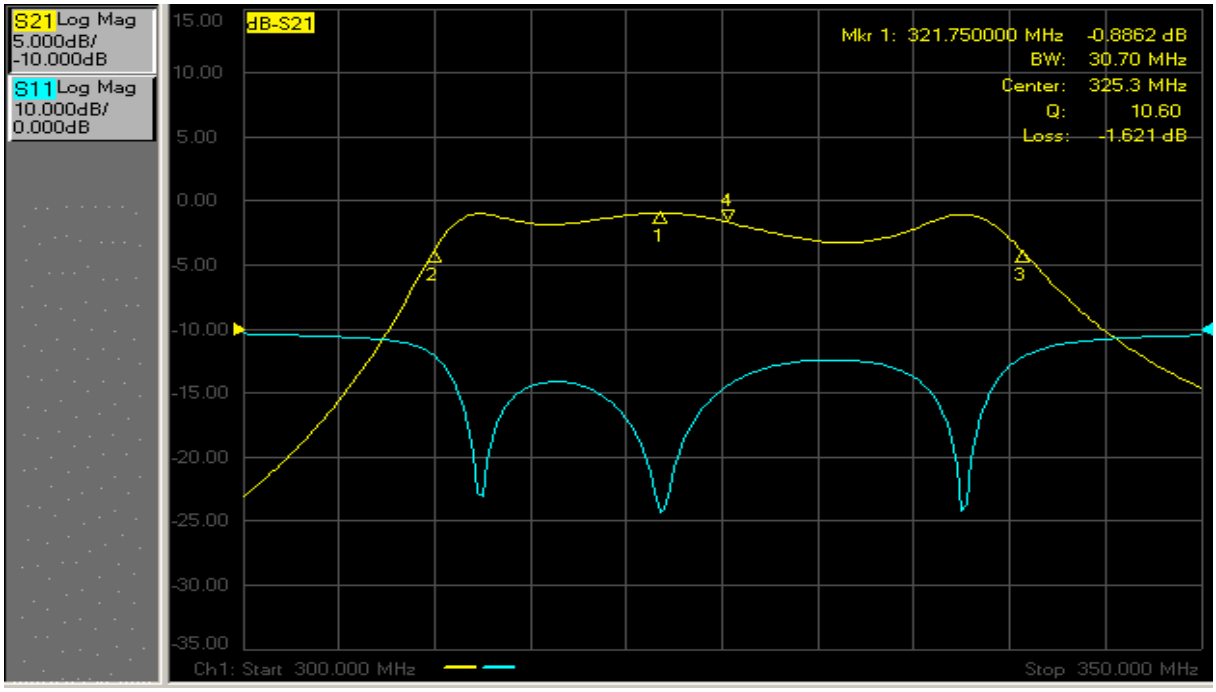

Figure 3.1.2.3.7 Measured frequency spectrum of the coupled RFD system.

the measured spectrum and the calculated one is very well. The bandwidth defined by -3dB level was 30.7 MHz, and the loaded Q-value was 10.6, almost the same as the single RFD. Figures 3.1.2.3.8 and 9 show the field amplitudes in the coupled RFD with a 30-kW input power. Although the coupled RFD system can save the required rf power by 50%, three demerits were observed:

1. the rising time of the second RFD is larger than the first one,
2. there is a rather long delay time in the second RFD excitation during the transient time, and
3. some rf mismatching between two RFD cavities was observed on the field shape.

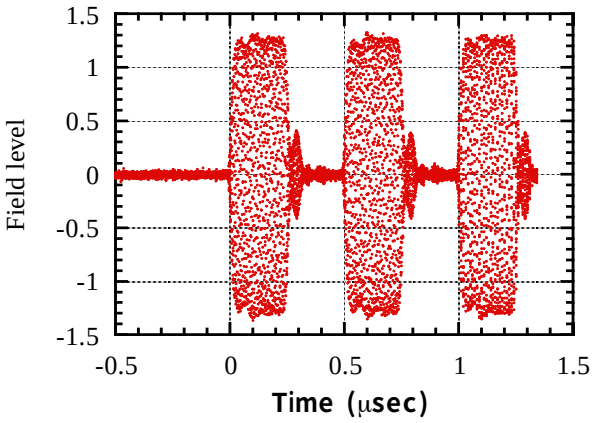

Fig. 3.1.2.3.8 RF field amplitude in the first cavity of the coupled RFD with a 30-kW input power.

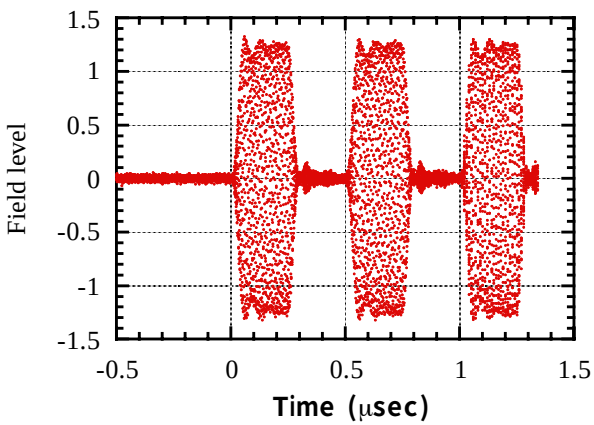

Fig. 3.1.2.3.9 RF field amplitude in the second cavity of the coupled RFD with a 30-kW input power.

It can be predicted that the effects mentioned above decrease the total efficiency of the deflection produced by two RFD cavities. The first decreases the total rising time, while the second implies that there are a few micro bunches which receive the deflection field from the first RFD only. The final rf driving system (single RFD drive or coupled RFD drive) will be carefully determined based on the knowledge obtained by both a chopped-beam test in the MEBT at KEK and the results of a precise simulation.

3. 1. 2. 3. 3 Scraper

A chopped bunch is scraped by a scraper, positioned 70 cm downstream from the RFD. The head of the scraper is made of a tungsten plate deposited on a copper plate for heat conduction. It is cooled by water. The horizontal position of the scraper head can be controlled with an accuracy of within 0.1 mm over a length of 50 mm. The beam current into the scraper can be measured with the required time resolution. A detailed thermal analysis shows that the maximum average temperature rise at the beam spot during normal operation is about 270 degrees.

3. 1. 2. 3. 4 Beam monitors

All monitors installed in the MEBT1 are listed in Table 3.1.2.3.3. Details are described in section 3.1.5.

Table 3.1.2.3.3 Beam monitors in the MEBT1.

Current monitor (CT)	4
Fast current monitor (FCT)	3
Beam position monitor (BPM)	8
Profile monitor (PM)	4
Emittance monitor (EM)	1
Bunch length monitor (BL)	1
Beam scraper	1
Beam stopper	1

3. 1. 2. 3. 5 Magnets for the MEBT1

Introduction

The medium-energy beam transport (MEBT1) line from RFQ to DTL was designed by using the Trace 3D code [1]. The MEBT1 comprises eight quadrupole (Q) magnets, one energy-analyzing (bending) magnet, two chopper cavities and two buncher cavities (Fig. 3.1.2.3.10). Since the longitudinal space is limited, as can be seen from Fig. 3.1.2.3.10, magnets of shorter length are desirable. On the other hand, the bore diameter of the Q-magnets should be chosen to be as large as possible compared with the beam diameter in order to avoid beam losses. Here, the calculated maximum beam diameter was about 20 mm in the MEBT1, where no alignment error was included. The parameters of the Q-magnets and bending magnet are shown in Table 3.1.2.3.4 and Table 3.1.2.3.5.

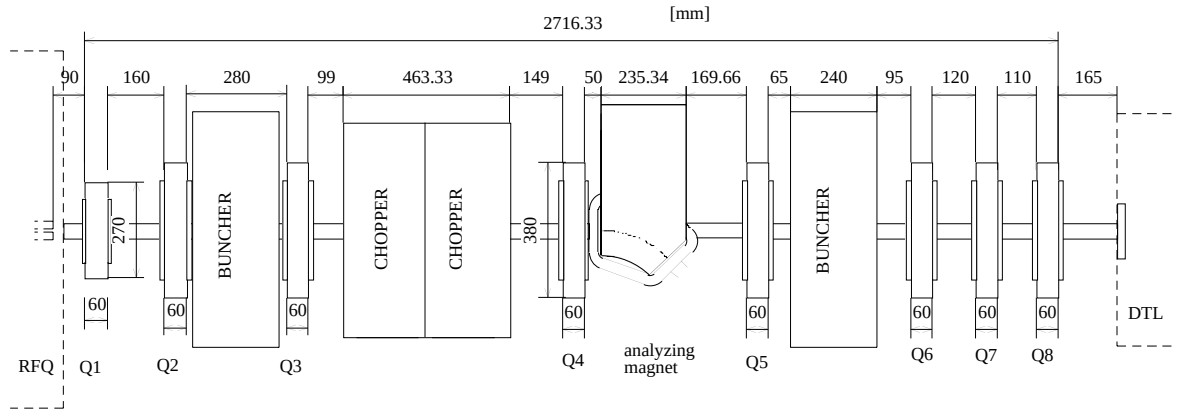

Fig. 3.1.2.3.10 Layout of the components in MEBT1.

Table 3.1.2.3.4 Parameters of the MEBT1 focusing magnets.

		Q1	Q2,Q3,Q6,Q7,Q8	Q4,Q5
Integrated field: GL	[T]	2.25	1.14〜1.92	0.780〜0.786
Maximum GL	[T]	3.54	2.39(Q3,Q6=1.74)	1.14
Maximum field: (G)	[T/m]	46.7	31(Q3,Q6=22.6)	14.1
Effective length	[mm]	75.8	77.0	80.9
Core length	[mm]	60	60	60
Aperture diameter	[mm]	30	41	52
Turn number of coil	[turn/pole]	15	19	19
Coil (hollow-conductor) size	[mm]	4×4,t=0.8	5×6,t=1.0	5×6,t=1.0
Max current (DC)	[A]	300	300(Q3,Q6=200)	200
Resistance	[mΩ]	30.5	25.3〜25.9	25.4, 25.9
Voltage	[V]	9.7	7.9(Q3,Q6=5.3)	5.3
Water flow rate	[Liter/min]	2.8	2	2
Maximum water temperature rise	[℃]	11	15.7(Q3,Q6=7)	7
Water pressure drop	[MPa]	0.21	0.22	0.22

Table 3.1.2.3.5 Parameters of the energy-analyzing magnet.

Beam energy	[MeV]	3
Integrated field (MAX)	[T • m]	0.1961(0.2787)
Magnetic field	[T]	0.7388
Effective length	[mm]	265.4
Core length	[mm]	235.3
Bend angle	[degree]	45
Radius of curvature	[mm]	262.82
Gap (shim gap)	[mm]	47.20(42.48)
Turn number of coil	[turn/pole]	72
Coil size	[mm]	6×6, t=1
Excitation current (MAX)	[A]	199.8(300)
Resistance	[mΩ]	103.02
Voltage	[V]	33.8
Water flow rate	[Liter/min]	6
Maximum water temperature rise	[℃]	25
Water pressure drop	[MPa]	0.39

Structure features

In order to measure the transverse beam position and the beam width, eight beam-position monitors (BPM), attached into a short vacuum duct, were installed in the bore holes of the Q-magnets. Thus, the shape of the pole-tips were carefully designed and fabricated for satisfying the requirements. Furthermore, five sets of steering coils were wound around the yoke of five Q-magnets. The C-type dipole magnet was chosen for analyzing the RFQ beam. Cross-sectional views of the magnets are shown in Fig. 3.1.2.3.11 and Fig. 3.1.2.3.12.

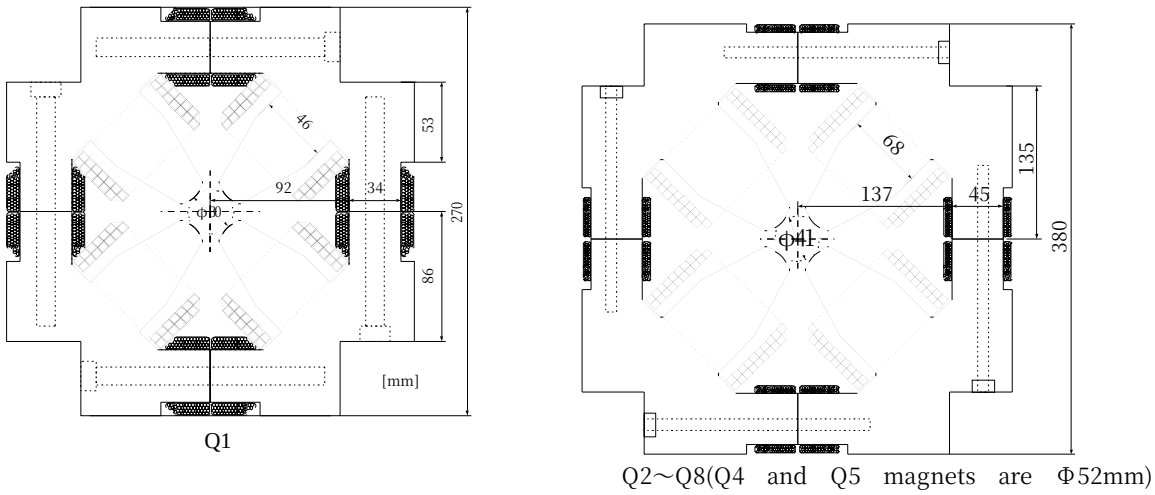

Fig. 3.1.2.3.11 Cross-sectional view of the quadrupole magnets.

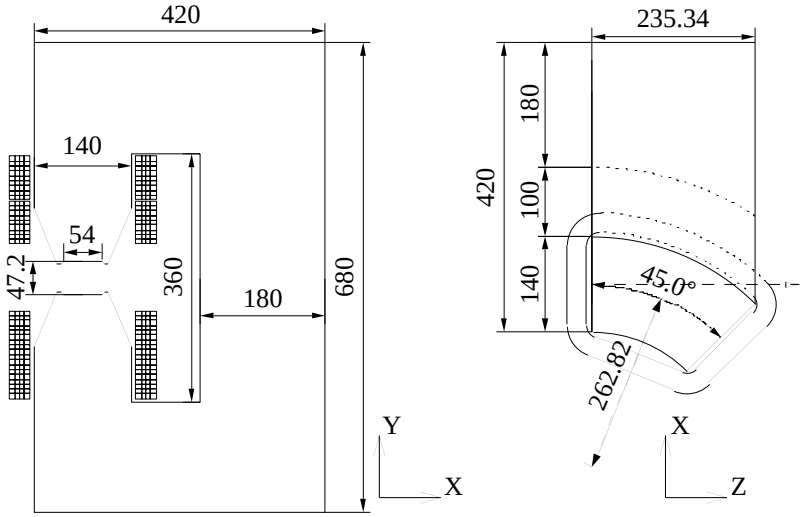

Fig. 3.1.2.3.12 Cross-sectional view of the energy analyzing magnet.

Magnetic field analysis

In order to achieve a magnetic field gradient with a uniform distribution, the shape of the magnetic poles was optimized based on the two and three-dimensional codes (POISSON and MAFIA). Figure 3.1.2.3.13 shows the radial distribution of the integrated field with the design current. The integrated field is uniform within 0.2% over the radial region from the beam axis to the aperture radius of a beam duct.

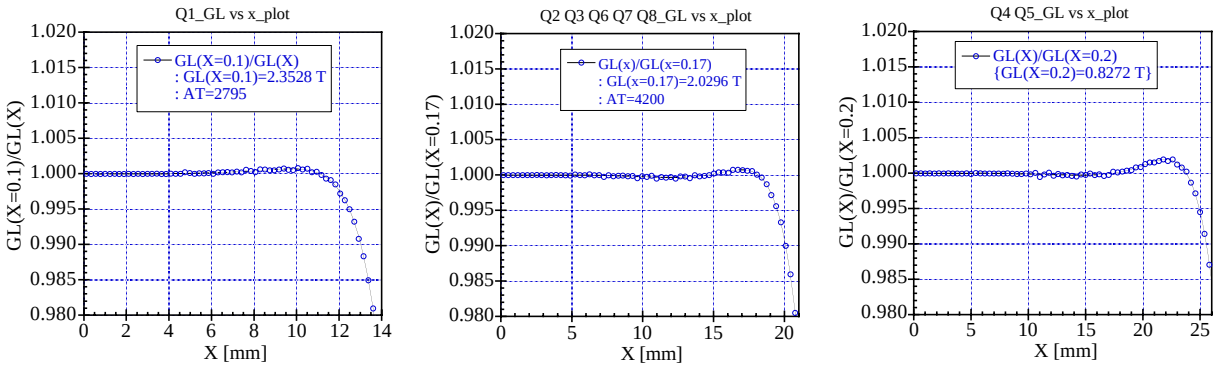

Fig. 3.1.2.3.13 Calculated radial distribution of the integrated field for all Q-magnets with the design current.

Results of the measurements

We measured the higher order multipole components of the Q-magnets by a rotating coil. Figure 3.1.2.3.14 shows the measured multipole components at the magnetic center near the design current. Both the dipole and multipole components are less than 0.2% of the quadrupole one. It can be said that the higher order multipole components are rather small at

the magnetic center. Figure 3.1.2.3.15 shows the measured deviation of the magnetic field center from the mechanical center near the design current. The deviation of the magnetic center from the mechanical one for all quadrupole magnets (except for the first one) are sufficiently small, satisfying the required accuracy. Figure 3.1.2.3.16 shows the excitation curve of the bending magnet measured by using a Hall probe. A beam energy of 3 MeV corresponds to an excitation current of about 200 A.

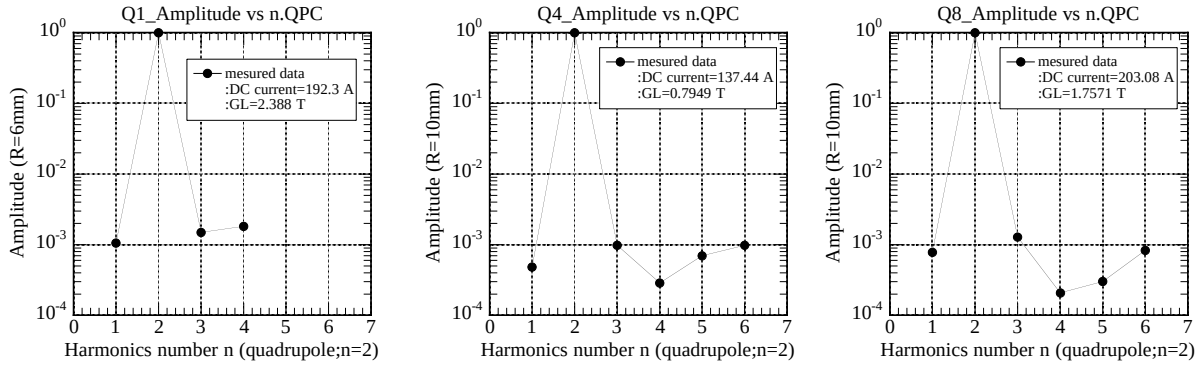

Fig. 3.1.2.3.14 Measured multipole components at the magnetic field center near the design current.

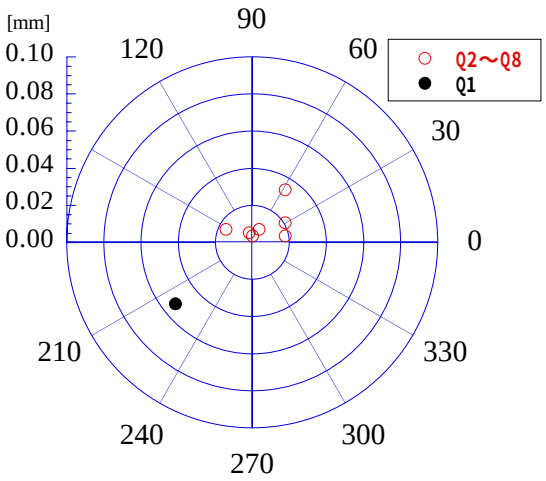

Fig. 3.1.2.3.15 Measured deviation of the magnetic field center from the mechanical one near the design current.

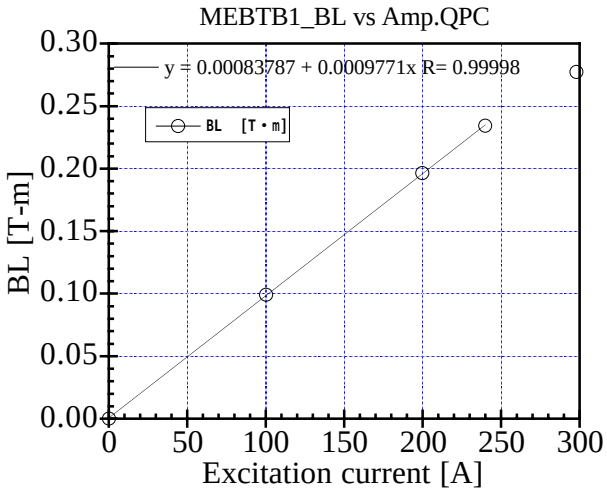

Fig. 3.1.2.3.16 Excitation curve of the bending magnet measured by a Hall probe.

3. 1. 2. 3. 6 Alignment

The specified accuracies for the alignment of each component in the MEBT1 are as follows:

transverse magnet position ±0.05 mm,
transverse rf cavity position ±0.1 mm and
longitudinal position ±0.1 mm.

The alignment was performed by using three templates for a position measurement, which could be set at the entrance, the mid position and the exit of the MEBT rack within an accuracy of ±20 μm. At first, the beam axis was determined by setting two templates with optical targets, which determine the beam axis to the standard corner on the MEBT rack. Then, the mechanical centers of the magnets, specified by the optical target in the magnet's bore, were aligned on the beam axis. The position of the magnets was gradually tuned by using thin shims and standard pins. The alignment between the RFQ and the MEBT was done by using optical targets on the templates: the horizontal position of the targets is away from the beam axis by 70 cm. The final measured alignment accuracies are as follows:

1. the maximum deviation between the beam axis and the bore center of each magnet is less than 20 μm and
2. the slope of horizontal and vertical directions between the alignment axes of RFQ and MEBT are less than the limit of the measurement accuracy and 7 μm/m, respectively.

The optical target on the side position of the template can be replaced by a laser target (section 3.1.2.8), which will be utilized in the overall alignment of the 400-MeV linac.

3. 1. 2. 3. 7 Beam test

A first beam test of the MEBT was successfully performed. Since the peak current is about 10 mA, some tunings of the focusing magnets for the 50-mA design values were required. A transmission ratio of nearly 100% was easily achieved, showing that the fundamental fabrication and alignment of the MEBT were successfully finished. A detailed beam study with a high peak current is planned for studying the beam behavior with strong space-charge effects, which seems to be crucial to the success of high-intensity proton acceleration.

A chopped-beam experiment was performed. The chopped beam was observed by five kinds of monitors, current monitors (CT), fast current monitors (FCT), beam-position monitors (BPM), a beam scraper and a Faraday cup. A low average beam power (a 5-mA peak current, a beam-pulse width of 50 μsec, a repetition rate of 5 Hz) was used. Figure 3.1.2.3.17 shows the measured signal of a chopped beam pulse from one of the electrode of BPM installed into Q8 (the last quadrupole magnet in the MEBT). The coupled chopper cavity was driven with an rf power of more than 30 kW and a chopping frequency of 2 MHz. A beam scraper position of 8 mm away from the beam center axis was chosen, since there is no scraped particles for the normal beam. Four or five micro bunches were observed during transient times of the chopped beam.

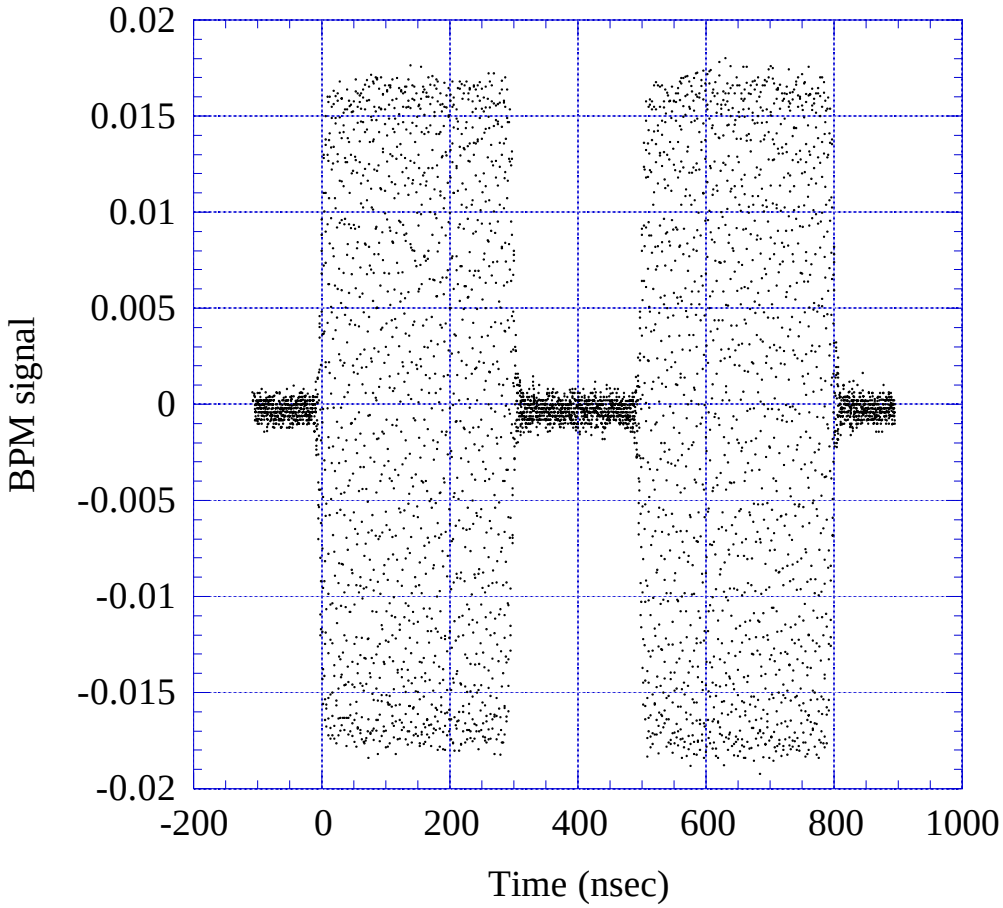

Figure 3.1.2.3.17 Measured signal of a chopped beam pulse from one of the electrode of the beam position monitor installed into Q8 (the last quadrupole magnet in the MEBT).

References

[1] JHF Project Office, "JHF Accelerator Design Study Report", KEK Report 97-16 Chapter 4 (JHF-97-10), 1998.

[2] S. Fu and T. Kato, "Design study on a medium-energy beam-transport line for the JHF proton linac," NIM **A 457** (2001) 423.

[3] T. Kato, New Design of an RF Beam Chopper, Proc. of 7th Symp. on Acc. Sci. & Tech. (1989) 288.

[4] S. Fu and T. Kato, "RF-chopper for the JHF proton linac," NIM **A 440** (2000) 296.